Chinese Journal of Physics 56 (2018) 783–792

Contents lists available at ScienceDirect

Chinese Journal of Physics

journal homepage: www.elsevier.com/locate/cjph

Investigation of structural and electronic properties of β- HgS: Molecular dynamics simulations

Cihan Kürkçü[a], Selgin AL[b,*], Ziya Merdan[c], Çağatay Yamçiçier[d], Hülya Öztürk[b]

[a] Vocational School of Technical Sciences, Ahi Evran University, Kirsehir 40100, Turkey
[b] Faculty of Arts and Sciences, Ahi Evran University, Kirsehir 40100, Turkey
[c] Science Faculty, Gazi University, Ankara, Turkey
[d] Institute of Science, Gazi University, Ankara, Turkey

ARTICLE INFO

Keywords:
β-HgS
Molecular dynamics simulations
Intermediate states
Structural phase transitions

ABSTRACT

The pressure induced phase transition of β-HgS is studied using an ab initio molecular dynamics simulation. The structural phase transformation from the zinc-blende structure to the NaCl-type structure (space group $Fm\bar{3}m$) and from this structure to CsCl-type structure ($Pm\bar{3}m$) with the application of hydrostatic pressure is predicted. Additionally, the electronic properties of HgS and various physical properties such as the lattice constants, the bulk modulus and the pressure derivative of the bulk modulus are revealed. Furthermore, these phase transitions are obtained using the total energy and enthalpy calculations. According to these calculations these transformations are occurring at about 20 GPa and 28 GPa for $F\bar{4}3m \rightarrow Fm\bar{3}m$ and $Fm\bar{3}m \rightarrow Pm\bar{3}m$, respectively.

1. Introduction

HgS (mercuric sulfide) is a well-known semiconductor from the II to VI family which has gained a lot of interest by the researchers due to its potential to be used in infrared sensors, optoelectronic and telecommunication devices [1,2]. HgS presents two different structures at ambient conditions, namely; alpha- HgS (α- HgS) and beta-HgS (β-HgS). α-HgS phase or cinnabar is red and represents a hexagonal crystal structure with a space group of $P3_121$ with a band gap of 2.1 eV under ambient conditions [3,4]. β-HgS or metacinnabar is black and has a zinc blende structure with a space group of $F\bar{4}3m$.

The pressure induced phase transition of α-HgS from cinnabar to NaCl structure (rock salt) was determined by Huang and Ruoff [5] at about 13 GPa by energy dispersive X-ray diffraction method. On the other hand, Werner et al. [6] and Joy et al. [7] reported no phase transition for α-HgS from cinnabar structure up to 20 GPa and 15 GPa, respectively, by using high pressure X-ray diffraction. The DFT (density functional theory) calculation showed a phase transition to rock salt at about 24 GPa [8] while Sun and Dong's [9,10] first principle computation suggested about 27 GPa transition pressure. Yang et al. [4] reported a phase transition of β-HgS from zinc blende (space group $F\bar{4}3m$) to cinnabar (space group $P3_121$) then to rock salt (space group $Fm\bar{3}m$) at 3.4 and 14.3 GPa using first principles calculations. Recently, HgS has been proposed to utilize as an electron acceptor in hybrid solar cells [11]. Galain et al. synthesized HgS via hydrothermal method and only obtained α-HgS and β-HgS.

A number of methods have been applied to reveal the structural phase transitions of mercury chalcogenides. The experimental methods that were adapted in literature such as resistivity, conductivity and spectroscopic measurements are limited. For instance, conductivity or resistivity measurements can be performed up to 20 GPa which leaves the properties of HgS unrevealed above 20 GPa

* Corresponding author.
E-mail address: selgin.al@ahievran.edu (S. AL).

https://doi.org/10.1016/j.cjph.2018.03.008
Received 13 February 2018; Received in revised form 24 February 2018; Accepted 19 March 2018
Available online 21 March 2018

[8]. The calculations and simulations of phase transitions under high pressure by using suitable techniques enable to overcome these limitations and give information about unexplored properties of the material. The increasing importance of HgS, variations in results and limitations of experiments directed us to study HgS further. Thus, in the present study, the pressure induced structural phase transitions of HgS with ab initio calculations are performed up to 60 GPa. The electronic, structural and physical properties of HgS are investigated. The ab initio total energy calculations are carried out. Results demonstrate that the structural transitions follow a zinc blende to rock salt (NaCl-type structure, space group $Fm\bar{3}m$), then to CsCl-type structure (space group $Pm\bar{3}m$) pattern under hydrostatic pressure.

2. Method of computation

The calculations were carried out by using ab initio program SIESTA [12]. This is placed on first principles calculations within the density functional theory method. The exchange-correlation energy was calculated by using the generalized gradient approximation of Perdew–Burke–Ernzerhof (PBE) [13]. The self-consistent "norm-conversing" pseudopotentials were achieved by using the Troullier–Martins scheme [14]. In the calculations, double-zeta polarized orbitals were applied for a real space grid. A cutoff energy of 350 Ryd was used in all calculations. The simulation cell consisted of 64 atoms with periodic boundary conditions. The Γ-point sampling for the Brillouin-zone integration was employed. The Brillouin-zone integration was performed with 8 × 8 × 8 k-point mesh for all phases of HgS following the convention of Monkhorst and Pack [15]. These k-point meshes were utilized for the energy–volume calculations. Parrinello and Rahman [16] method was used to apply external pressure to the system. Pressure was increased with an increment of 5 GPa. The structures were allowed to relax and find their equilibrium volumes and lowest energies for each value of the applied pressure by optimizing their lattice vectors and atomic positions. Geometries were relaxed until the forces on all atoms were less than 0.01 eV $Å^{-1}$ and the stress tolerances were getting less until 0.5 GPa. In order to analyze each MD time step, the KPLOT program and RGS algorithm [17,18] were considered which gives elaborated knowledge about cell parameters, atomic positions and space group of an analyzed structure.

3. Results

The calculations of equilibrium lattice parameters of the zinc-blende phase of HgS are performed initially by relaxing 64 atoms supercell at zero pressure. Then the results are compared to available experimental and theoretical data in the literature. The equilibrium unit cell lattice constant is found to be $a = 6.0428$ Å. This value is in a reasonable range with previously reported experimental ($a = 5.8310$ Å [19]) and theoretical data ($a = 5.8310 - 6.1920$ Å [20–25]).

In order to determine the phase transition of HgS, the pressure-volume relation is obtained by using the constant pressure ab initio simulation. The *P–V* curve is given in Fig. 1. A sharp change is observed in volume as the pressure increases from 10 GPa to 20 GPa and from 50 GPa to 60 GPa as shown in Fig. 1. This indicates a first order pressure induced phase transition in HgS.

Fig. 2 exhibits the structural analysis of HgS where zinc-blende structure converts into a NaCl-type structure at 20 GPa and then this structure transforms to a CsCl-type structure at 60 GPa and their equilibrium lattice parameters and the atomic fractional coordinates that are summarized in Table 1. The results suggest that molecular dynamics simulations can successfully generate phase transitions of HgS under high pressure. However, the calculated phase transition pressures are slightly higher than the experimental values. This is due to using a defect free structure with a finite volume where the phase transition occurs over the whole simulation cell instead of nucleation and buildup. Thus, when the particular conditions such as finite size of the simulation cell, the time scale of

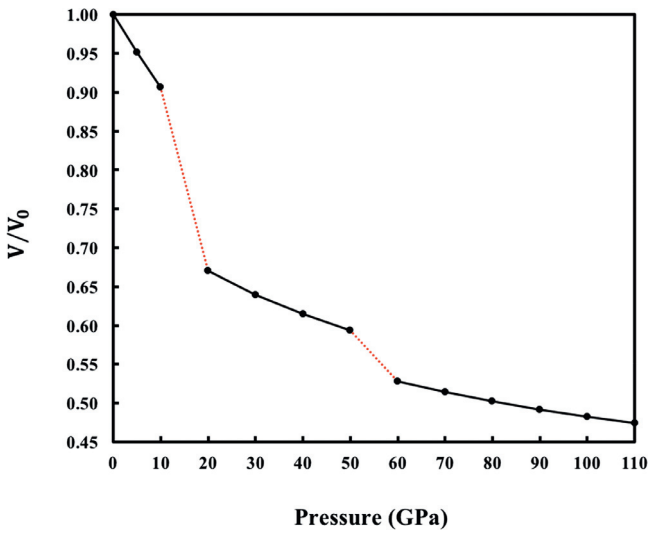

Fig. 1. The volume change as a function of pressure.

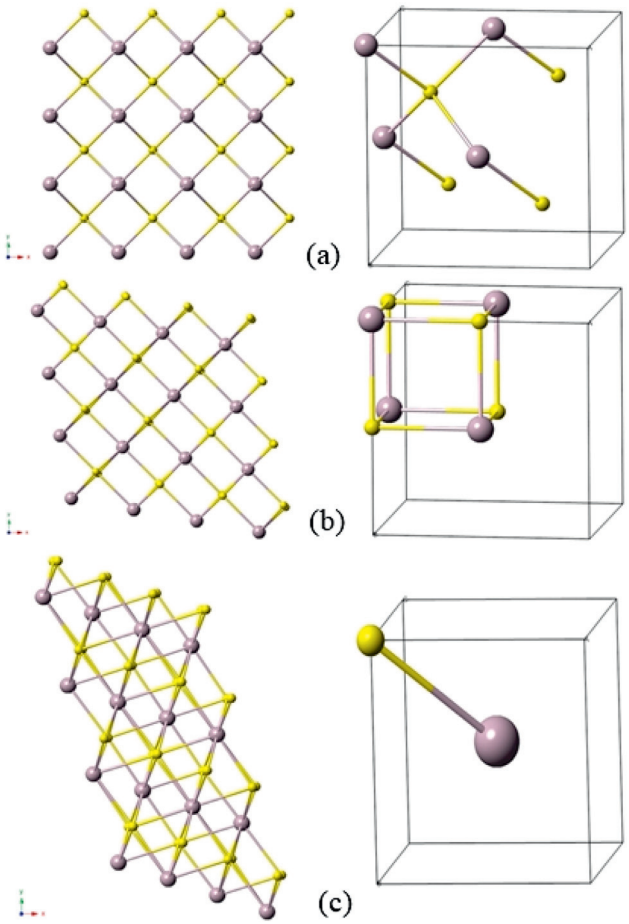

Fig. 2. Crystal structures of β-HgS: zinc-blende structure (a) at zero-pressure, NaCl structure (b) at 20 GPa, and CsCl structure (c) at 60 GPa.

Table 1
The equilibrium lattice parameters and the atomic fractional coordinates of the $F\bar{4}3m$, $Fm\bar{3}m$ and $Pm\bar{3}m$ phases.

Phases	a (Å)	b (Å)	c (Å)	x	y	z
$F\bar{4}3m$	6.0428	6.0428	6.0428	Hg: 0.0000	0.0000	0.0000
				Hg: 0.0000	0.5000	0.5000
				Hg: 0.5000	0.5000	0.0000
				Hg: 0.5000	0.0000	0.0500
				S: 0.2500	0.2500	0.2500
				S: 0.2500	0.7500	0.7500
				S: 0.7500	0.7500	0.2500
				S: 0.7500	0.2500	0.7500
$Fm\bar{3}m$	5.5861	5.5861	5.5861	Hg: 0.0000	0.0000	0.0000
				Hg: 0.0000	0.5000	0.5000
				Hg: 0.5000	0.5000	0.0000
				Hg: 0.5000	0.0000	0.5000
				S: 0.5000	0.5000	0.5000
				S: 0.5000	0.0000	0.0000
				S: 0.0000	0.0000	0.5000
				S: 0.0000	0.5000	0.0000
$Pm\bar{3}m$	3.4322	3.4322	3.4322	Hg: 0.5000	0.5000	0.5000
				S: 0.0000	0.0000	0.0000

simulations, etc. are considered, such an overestimated transition pressure is anticipated [26]. In order to avoid this situation, energy–volume calculations are considered to study the stability of zinc-blende, NaCl and CsCl-type structures since the thermodynamic theorem does not take into account the possible existence of such an activation energy barrier separating the two structural phases. The result is presented in Fig. 3. As can be seen in Fig. 3, the most stable phase of HgS is $F\bar{4}3m$.

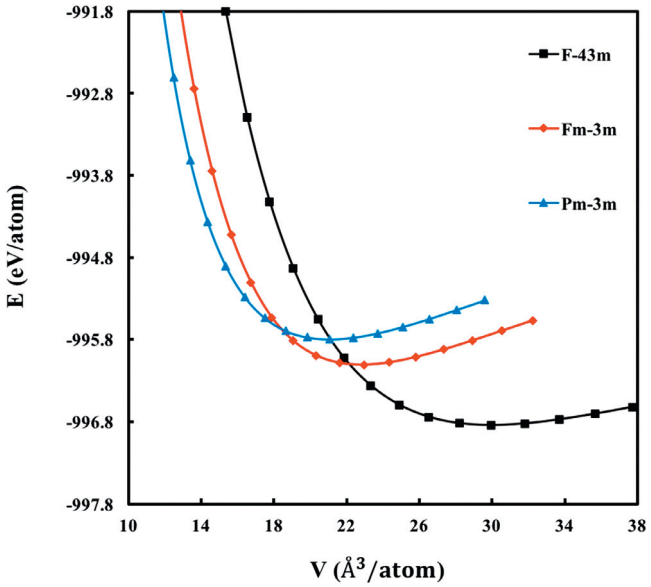

Fig. 3. The total energy of β-HgS as a function of volume.

Their energy–volume data is fitted to the third-order Birch–Murnaghan equation of state [27,28] that given by

$$P = 1.5B_0\left[(V/V_0)^{-\frac{7}{3}} - (V/V_0)^{-\frac{5}{3}}\right]x\left\{1 + 0.75(B_0' - 4)\left[(V/V_0)^{-\frac{2}{3}} - 1\right]\right\} \quad (1)$$

where P is the pressure, V is the volume at pressure, V_0, B_0 and B_0' are the volume, bulk modulus and its pressure derivate at 0 GPa, respectively.

At the phase transition, the two phases have the same enthalpy ($H = E_{tot} + PV$, where $P = -dE_{tot}/dV$ is obtained by direct differentiation of the calculated the energy–volume curves), therefore the transition pressure can be easily determined by equating the enthalpy of the two pressure is shown in Fig. 4. A transition pressure of about 20 GPa is obtained for $F\bar{4}3m \rightarrow Fm\bar{3}m$ and about 28 GPa for $\bar{3}m \rightarrow Pm\bar{3}m$, which is comparable with the experimental and theoretical results [22,25,29] and the equilibrium lattice parameters, equilibrium volume rates, bulk modulus and their pressure derivatives, together with the other theoretical and experimental data for all structures of HgS are reported in Table 2.

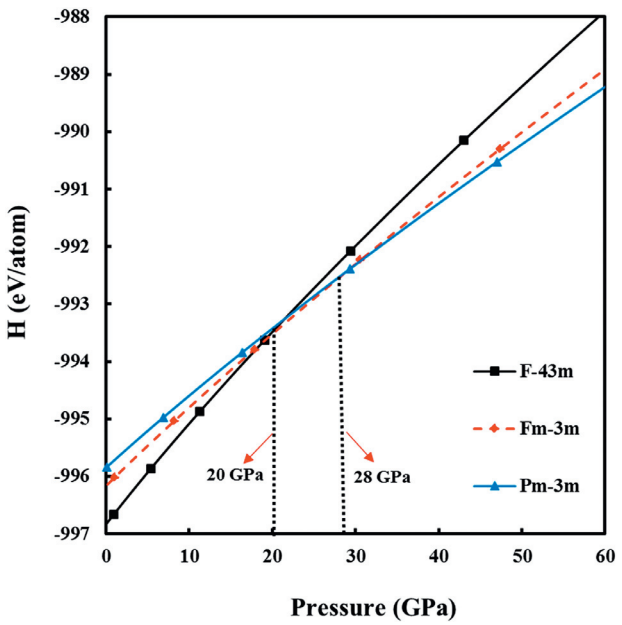

Fig. 4. The enthalpy curve of β-HgS as a function of pressure.

Table 2
Theoretical ($T = 0$ K) lattice parameters of HgS for zinc-blende structure (space group, SG: $F\bar{4}3m$) and high-pressure phases: Rock salt structure (SG: $Fm\bar{3}m$) and CsCl structure (SG:$Pm\bar{3}m$) with GGA at the corresponding pressure P_T. *a, b*, and *c* are the lattice parameters, *V* is the equilibrium volume at the respective pressure, B_0 the bulk modulus, $B_0^{'}$ the first derivative of the bulk modulus.

Phases	P_T (GPa)	*a* (Å)	*b* (Å)	*c* (Å)	*V* (Å^3)	B_0 (GPa)	B_0'	References
F*$\bar{4}$*3m	0	6.0428	6.0428	6.0428	55.16	59.08	4.69	This study
		6.0090	6.0090	6.0090	54.67	50.40	4.90	[20]
		6.1920	6.1920	6.1920	59.35	47.90	4.70	[20]
		6.0030	6.0030	6.0030	54.80	67.00		[21]
		5.8800	5.8800	5.8800		68.60	2.94	[22]
		5.8510	5.8510	5.8510				[19]
		6.0200	6.0200	6.0200		68.23		[23]
		6.1970	6.1970	6.1970		50.02		[23]
		5.9880	5.9880	5.9880		50.18	4.61	[24]
		5.9900	5.9900	5.9900		63.80	2.60	[25]
Fm*$\bar{3}$*m	20	5.5861	5.5861	5.5861	43.57	98.91	4.65	This study
	19.9	5.4600	5.4600	5.4600		86.28		[22]
	16.1	5.5700	5.5700	5.5700		67.09	4.76	[25]
	3.6	5.8530	5.8530	5.8530				[29]
Pm*$\bar{3}$*m	28	3.4322	3.4322	3.4322	31.65	94.31	5.44	This study
		3.5230	3.5230	3.5230	43.73	67.40	4.80	[20]

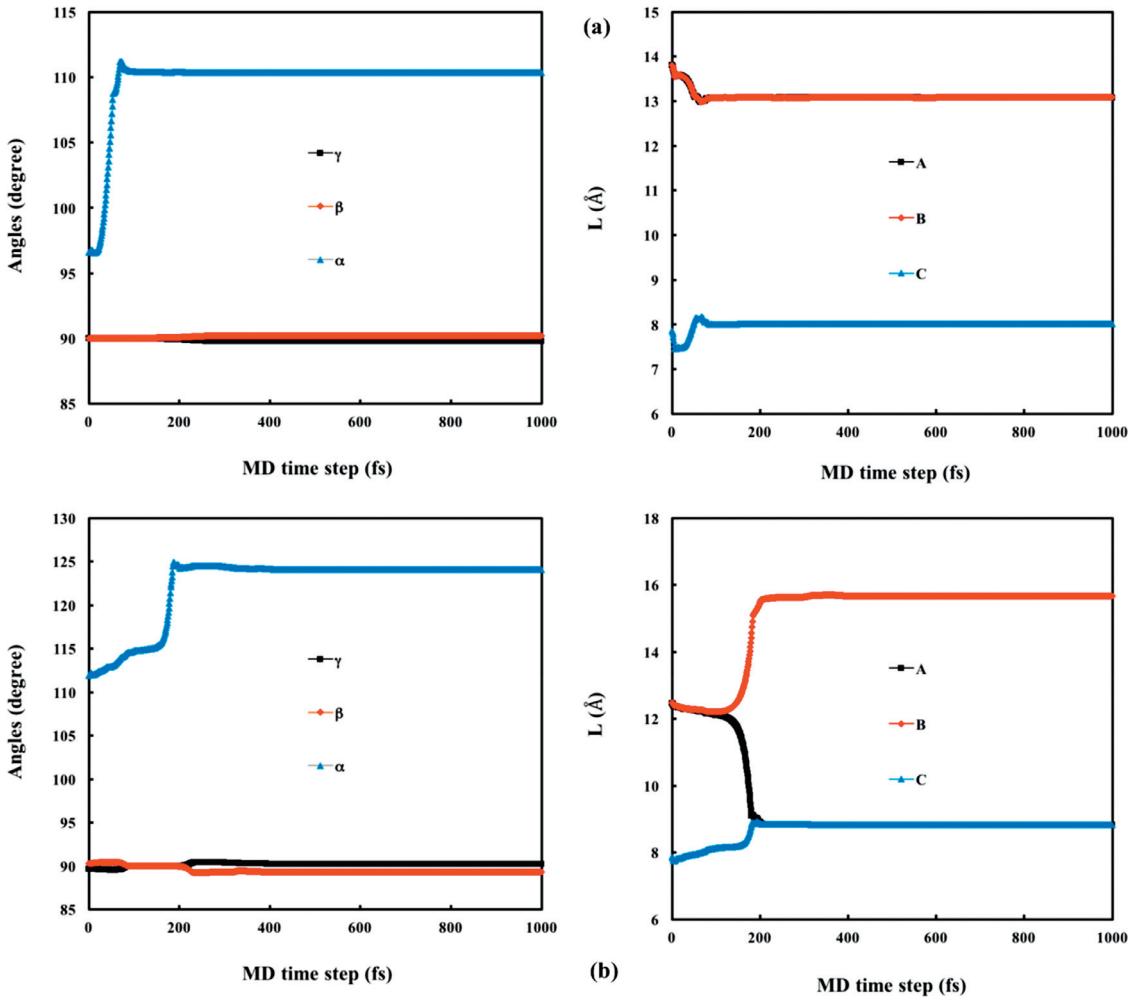

Fig. 5. The angles and simulation cell lengths as a function of MD time step: (a) NaCl structure at 20 GPa and (b) CsCl structure at 60 GPa.

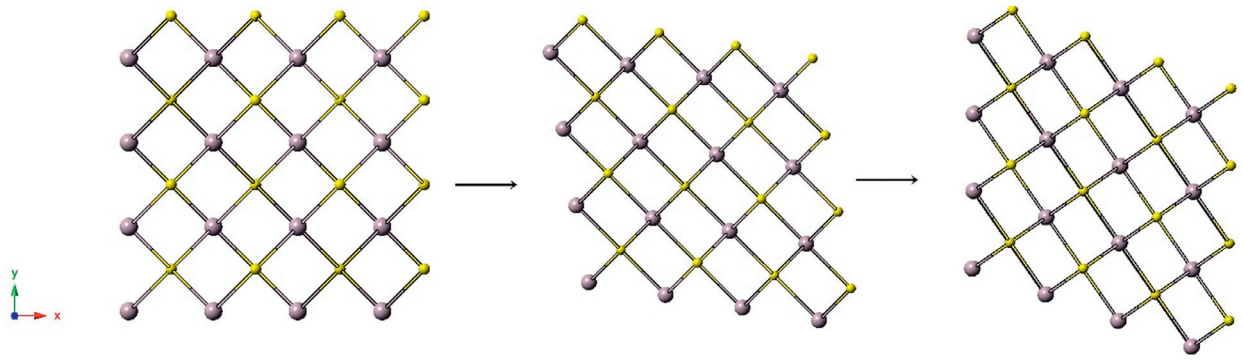

Fig. 6. At 20 GPa, evolution of the $Fm\bar{3}m$ phase at MD Time steps.

The modification of simulation cell during the phase change reveals important information about the mechanism of this transformation at the atomistic level and hence as a next step we study the variation of the simulation cell lengths and angles as a function of MD time step and the results are plotted in Fig. 5. The simulation box is initially a cubic cell whose lattice vectors are along the [0 0 1], [0 1 0] and [0 0 1] directions, respectively. The magnitude of these vectors is plotted in the figure.

As shown in Fig. 5 a, as the β and γ angles remain constant throughout the simulation, the alpha angle starts to increase at around 100 fs, and after reaching 110°, it remains unchanged. Simulation cell lengths also experience small changes up to about 100 fs and remain constant throughout the simulation.

In Fig. 5 b, while gamma and beta angles are stable at about 90°, the alpha angle increases at about 200 fs and reaches 125°. Simulation cell lengths remain constant up to 200 fs and there is no significant change in C length. The length A shortens to approximately 8.5 Å while the length B stretches to about 16 Å.

In order to characterize any intermediate state(s) formed during the $F\bar{4}3m \rightarrow Fm\bar{3}m$ and $Fm\bar{3}m \rightarrow Pm\bar{3}m$ phase transformations of HgS, we carefully analyze the structure at each MD time step using the KPLOT program.

For the NaCl-type structure with space group $Fm\bar{3}m$ of HgS, we determine a cubic structure with $F432$ symmetry at 57 fs whose lattice parameters are $a = 3.4062$ Å, $b = 3.6396$ Å, $c = 3.6647$ Å. The cubic NaCl-structure having $Fm\bar{3}m$ symmetry forms at 60 fs.

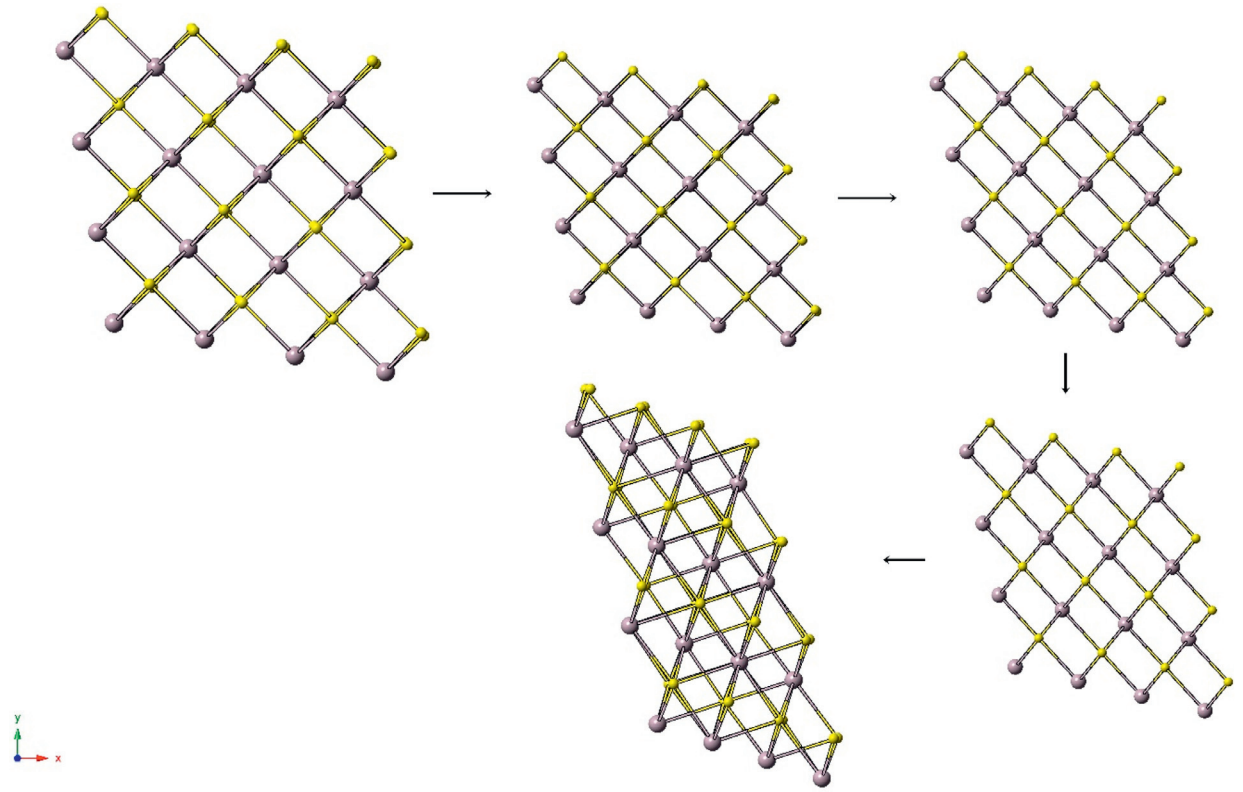

Fig. 7. At 60 GPa, evolution of the $Pm\bar{3}m$ phase at MD Time steps.

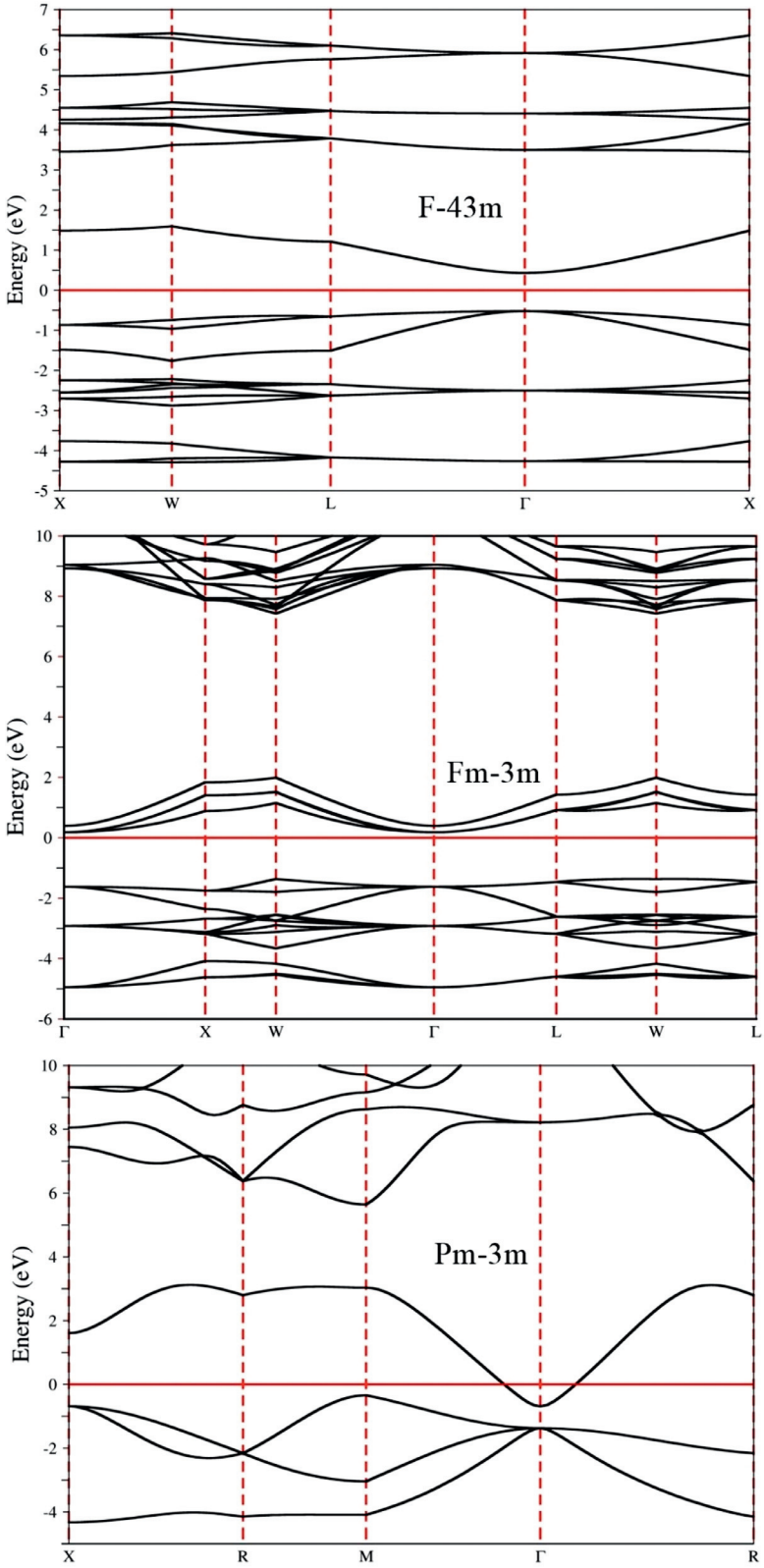

Fig. 8. Electronic band structures of β-HgS for $F\bar{4}3m$, $Fm\bar{3}m$ and $Pm\bar{3}m$ phases.

Table 3
The bond lengths of unit cells of the $F\bar{4}3m$, $Fm\bar{3}m$ and $Pm\bar{3}m$ phases. B_{min} and B_{max} indicate minimum and maximum bond lengths, respectively.

Phase	From	To	Bond lengths (Å)	
$F\bar{4}3m$	Hg	S	B_{min} = 2.690	B_{max} = 5.150
	Hg	Hg	4.392	
	S	S	4.392	
$Fm\bar{3}m$	Hg	S	B_{min} = 2.720	B_{max} = 4.712
	Hg	Hg	3.847	
	S	S	3.847	
$Pm\bar{3}m$	Hg	S	2.739	

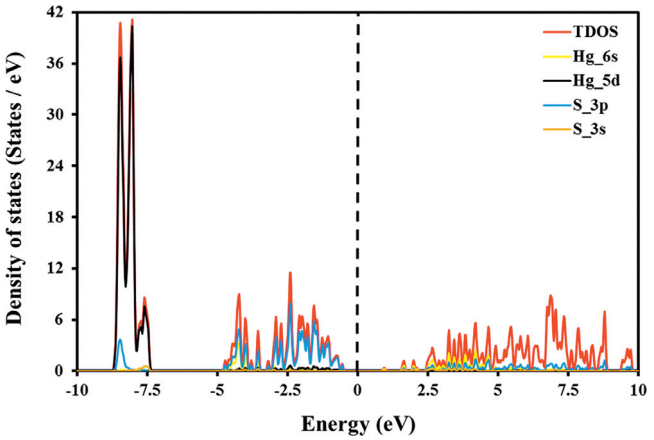

Fig. 9. The calculated partial density of states for zinc-blende structure.

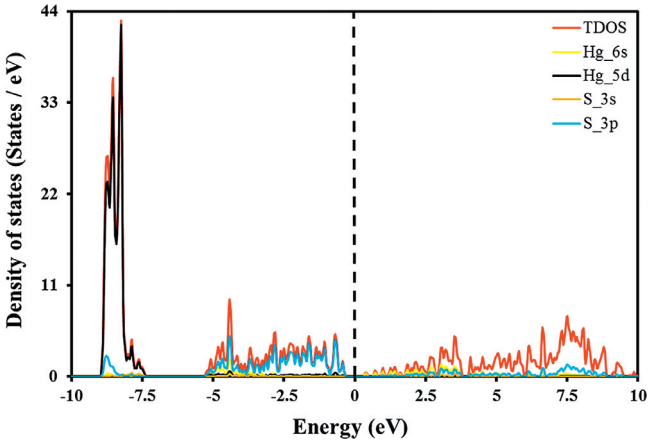

Fig. 10. The calculated partial density of states for NaCl structure.

This intermediate state(s) of $Fm\bar{3}m$ phase is depicted in Fig. 6.

For the CsCl-type structure with space group $Pm\bar{3}m$ of HgS, we determine a tetragonal structure with $I4/mmm$ symmetry at 36 fs whose lattice parameters are a = 4.1494 Å, b = 4.1494 Å, c = 4.3467 Å. In later time steps, we determine a monoclinic structure with $C2/m$ symmetry at 147 fs whose lattice parameters are a = 5.8972 Å, b = 4.0912 Å, c = 3.2581 Å and a trigonal structure with $R\bar{3}m$ symmetry at 160 fs whose lattice parameters are $a = b = c$ = 3.4409 Å. The cubic CsCl-structure having $Pm\bar{3}m$ symmetry forms at 183 fs. These intermediate state(s) of $Pm\bar{3}m$ phase are depicted in Fig. 7 and the bond lengths of unit cells of the $F\bar{4}3m$, $Fm\bar{3}m$ and $Pm\bar{3}m$ phases are reported in Table 3.

The computed electronic band structures (EBS) are given in Fig. 4 for $F\bar{4}3m$, $Fm\bar{3}m$ and $Pm\bar{3}m$ phases. Also total densities of states (TDOS) with partial densities of states (PDOS) of HgS are shown in Figs. 9–11 for zinc-blende-, NaCl- and CsCl-type structures, respectively. The DOS is calculated along high-symmetry directions and illustrated near the Fermi energy (E_F) level as a function of energy. Fermi level is set to be 0 eV. The symmetry points are X, W, L, Γ and X for $F\bar{4}3m$ phase, Γ, X, W, Γ, L, W and L for $Fm\bar{3}m$ phase and X, R, M, Γ and R for $Pm\bar{3}m$ phase. The EBS of HgS demonstrates that the valance band is located below the E_F level,

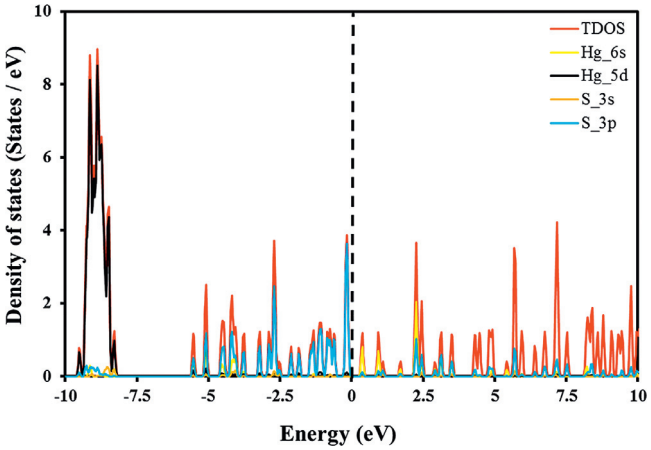

Fig. 11. The calculated partial density of states for CsCl structure.

whereas the conduction band is located above it.

The results point out that $F\bar{4}3m$ phase of HgS corresponds to a direct band transition with a band gap of 0.98 eV [20] due to the fact that the valance band maxima and the conduction band minima lie on the same symmetry point ($\Gamma - \Gamma$). $Fm\bar{3}m$ phase of HgS corresponds to an indirect band transition with a band gap of 1.54 eV. This is seen between W-point (the valence band maxima) and Γ-point (the conduction band minima). The $F\bar{4}3m$ and $Fm\bar{3}m$ phases of HgS have energy gaps between valance band and conduction band. This means that both two phases of HgS show semiconductor characteristic. On the other hand, $Pm\bar{3}m$ phase of HgS has no band gap at Fermi level indicating having metallic properties.

We calculated the partial density of states (PDOS) to obtain further information about the electronic nature of HgS and depicted in Figs. 9–11. It can be seen from Figs. 9–11 that the largest contribution come from Hg-5d states between −10 eV and −5 eV, S-3p states between −5 eV and 0 eV and Hg-6s states between 0 eV and 5 eV for all phases of HgS.

4. Conclusion

In the present study, we investigated structural characterization, electronic properties and high pressure induced phase transition in HgS using an ab initio molecular dynamic simulation. The most relevant conclusions are summarized as follows:

(i) The calculated ground state properties of these compounds at ambient pressure are comparable with the available experimental and theoretical data.
(ii) Two first-order phase transitions are proposed for β-HgS. The first one is a zinc-blende to-cubic phase transformation. The second one is a cubic to cubic phase transformation.
(iii) The band structure calculations reveal that the zinc-blende structure (space group: $F\bar{4}3m$) of β-HgS is a direct band gap semiconductor and the cubic structure (space group: $Fm\bar{3}m$) of β-HgS is an indirect band gap semiconductor, while another cubic structure (space group: $Pm\bar{3}m$) of β-HgS is a metal.

References

[1] T.J. Hu, et al., In situ electrical resistivity and hall effect measurement of beta-hgS under high pressure, Chin. Phys. Lett. 32 (1) (2015) 3.
[2] T. Ren, et al., A surfactant-assisted photochemical route to single crystalline HgS nanotubes, J. Photochem. Photobiol. A 173 (1) (2005) 93–98.
[3] A.M. Hao, et al., A study of the electrical properties of HgS under high pressure, J. Phys.-Condens. Matter 19 (42) (2007) 9.
[4] X.C. Yang, et al., Study of electronic and elastic properties of beta-HgS under high pressure via first-principles calculations, Phys. Status Solidi C 8 (5) (2011) Wiley-VCH Verlag Gmbh: Weinheim.
[5] T. Huang, A.L. Ruoff, Pressure-induced phase-transition of HgS, J. Appl. Phys. 54 (9) (1983) 5459–5461.
[6] A. Werner, et al., High-pressure x-ray diffraction studies on HgTe and HgS to 20 GPa, Phys. Rev. B 28 (6) (1983) 3330–3334.
[7] K.M.F. Joy, N.V. Jaya, J.J. Zhu, Structural transformation in Pbs and Hgs nanocrystals under high pressure, Mod. Phys. Lett. B 20 (16) (2006) 963–970.
[8] V.V. Shchennikov, S.V. Ovsyannikov, Thermoelectric properties and phase transitions of II–VI semiconductors at high pressure, Phys. Status Solidi B 244 (1) (2007) 437–442.
[9] S.-R. Sun, Y.-H. Dong, The optical properties of HgS under high pressures, Solid State Commun. 138 (9) (2006) 476–479.
[10] S.R. Sun, et al., Electronic structures and metallization of HgS under high pressures: first principles calculations and resistivity measurements, Phys. Rev. B 73 (11) (2006) 4.
[11] I. Galain, et al., Hydrothermal synthesis of alpha- and beta-HgS nanostructures, J. Cryst. Growth 457 (2017) 227–233.
[12] P. Ordejón, E. Artacho, J.M. Soler, Self-consistent order-density-functional calculations for very large systems, Phys. Rev. B 53 (16) (1996) R10441-R10444.
[13] J.P. Perdew, K. Burke, M. Ernzerhof, Generalized gradient approximation made simple, Phys. Rev. Lett. 77 (18) (1996) 3865–3868.
[14] N. Troullier, J.L. Martins, Efficient pseudopotentials for plane-wave calculations, Phys. Rev. B 43 (3) (1991) 1993–2006.
[15] H.J. Monkhorst, J.D. Pack, Special points for Brillouin-zone integrations, Phys. Rev. B 13 (12) (1976) 5188–5192.
[16] M. Parrinello, A. Rahman, Crystal structure and pair potentials: a molecular-dynamics study, Phys. Rev. Lett. 45 (14) (1980) 1196–1199.
[17] R. Hundt, et al., Determination of symmetries and idealized cell parameters for simulated structures, J. Appl. Crystallogr. 32 (3) (1999) 413–416.
[18] A. Hannemann, et al., A new algorithm for space-group determination, J. Appl. Crystallogr. 31 (6) (1998) 922–928.

[19] O. Madelung, Semiconductors-Basic Data, Springer Science & Business Media, 2012.
[20] S. Biering, P. Schwerdtfeger, A comparative density functional study of the low pressure phases of solid ZnX, CdX, and HgX: trends and relativistic effects, J. Chem. Phys. 136 (3) (2012) 034504.
[21] A. Delin, T. Klüner, Excitation spectra and ground-state properties from density-functional theory for the inverted band-structure systemsβ-HgS, HgSe, and HgTe, Phys. Rev. B 66 (3) (2002).
[22] N. Ullah, et al., Phase transition, electronic and optical properties of mercury chalcogenides under pressure, Phase Transitions 87 (6) (2014) 571–581.
[23] F. Boutaiba, A. Zaoui, M. Ferhat, Fundamental and transport properties of ZnX, CdX and HgX (X = S, Se, Te) compounds, Superlattices Microstruct. 46 (6) (2009) 823–832.
[24] I. Düz, et al., First principles investigations of HgX (X= S, Se and Te), Arch. Mater. Sci. 6 (2016) 6.
[25] Saini, P., D. Ahlawat, and D. Singh, Structural, electronic and optical properties of HgS under pressure using FP-LAPW method. 2017.
[26] H. Öztürk, M. Durandurdu, High-pressure phases of ZrO2: An ab initio constant-pressure study, Phys. Rev. B 79 (13) (2009) 134111.
[27] F. Birch, Finite elastic strain of cubic crystals, Phys. Rev. 71 (11) (1947) 809–824.
[28] F. Murnaghan, The compressibility of media under extreme pressures, Proc. Natl. Acad. Sci. 30 (9) (1944) 244–247.
[29] J. Chelikowsky, High-pressure phase transitions in diamond and zinc-blende semiconductors, Phys. Rev. B 35 (3) (1987) 1174–1180.